

A major purpose of the Technical Information Center is to provide the broadest dissemination possible of information contained in DOE's Research and Development Reports to business, industry, the academic community, and federal, state and local governments.

Although a small portion of this report is not reproducible, it is being made available to expedite the availability of information on the research discussed herein.

CONF-831203--43

Los Alamos National Laboratory is operated by the University of California for the United States Department of Energy under contract W-7405-ENG-36

NOTICE
PORTIONS OF THIS REPORT ARE ILLISIBLE.
It has been reproduced from the best available copy to permit the broadest possible availability.

TITLE POLOIDAL FIELD SYSTEM DESIGN FOR THE ZT-H REVERSED FIELD PINCH EXPERIMENT

AUTHOR(S) Kurt F. Schoenberg, Robert F. Gribble, Theodore W. Linton, William R. Reass

SUBMITTED TO 10th Symposium on Fusion Engineering - Philadelphia, PA
December 5 - 9, 1983

DISCLAIMER

This report was prepared as an account of work sponsored by an agency of the United States Government. Neither the United States Government nor any agency thereof, nor any of their employees, makes any warranty, express or implied, or assumes any legal liability or responsibility for the accuracy, completeness, or usefulness of any information, apparatus, product, or process disclosed, or represents that its use would not infringe privately owned rights. Reference herein to any specific commercial product, process, or service by trade name, trademark, manufacturer, or otherwise does not necessarily constitute or imply its endorsement, recommendation, or favoring by the United States Government or any agency thereof. The views and opinions of authors expressed herein do not necessarily state or reflect those of the United States Government or any agency thereof.

By acceptance of this article the publisher recognizes that the U.S. Government retains a nonexclusive royalty-free license to publish or reproduce the published form of this contribution or to allow others to do so for U.S. Government purposes. The Los Alamos National Laboratory requests that the publisher identify this article as work performed under the auspices of the U.S. Department of Energy.

MASTER

Los Alamos Los Alamos National Laboratory
Los Alamos, New Mexico 87545

POLOIDAL FIELD SYSTEM DESIGN FOR THE ZT-40U
REVERSED FIELD PINCH EXPERIMENT

Kurt F. Schoenberg, Robert F. Gribble, Theodore W. Linton and William R. Reass

Los Alamos National Laboratory
Los Alamos, New Mexico 87545

Introduction

The poloidal field system in a reversed field pinch (RFP) provides two important functions. It induces the toroidal electric field that drives the plasma current over the duration of the discharge, and it provides the magnetic boundary conditions necessary for plasma equilibrium. In ZT-40U, this functional dichotomy is achieved by using two separate systems of coils. The equilibrium winding, which provides the vertical field and field index necessary for plasma equilibrium, and the magnetizing winding, which provides the flux swing and magnetic energy necessary to set up and maintain the discharge. A cross-sectional drawing and flux plot of the poloidal field system is shown in Fig. 1.

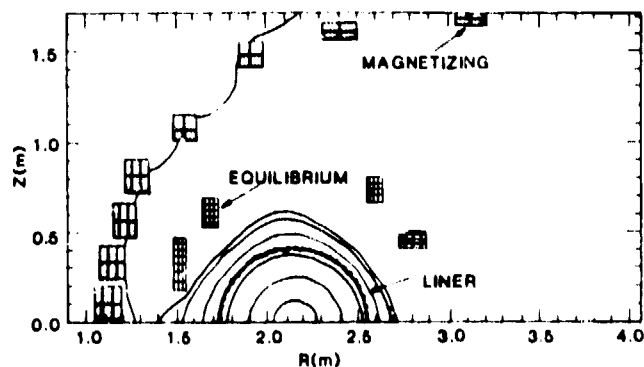


Fig. 1. A cross-sectional drawing and flux plot of the ZT-40U poloidal field system.

The main motivation behind the two coil system resides in the ability to inductively decouple the magnetizing and equilibrium windings. In principle, the decoupling greatly simplifies plasma equilibrium control since the equilibrium winding current and corresponding equilibrium vertical field are inductively driven by the plasma, and hence proportional to the plasma current. Corrections to the vertical field for fine tuning of the plasma equilibrium may then be accomplished by using modest trimming supplies. Thus, the experimental control of plasma current and plasma equilibrium are separable functions. Physically, the decoupling requires all magnetizing flux to completely link the equilibrium windings and plasma. That is, all magnetizing flux is spatially confined outside the equilibrium winding cage. This constraint also insures the minimization of stray magnetic fields in the plasma region.

Poloidal field system design is predicated on plasma/discharge performance. However, the design must also address secondary and mechanical constraints such as energy transfer efficiency, fabricability and accessibility after assembly. The interaction of these considerations comprises the design philosophy.

Equilibrium Specification

In ZT-40U, the plasma is contained inside a metallic vacuum vessel, that is nested within a conducting shell. The shell incorporates both a

toroidal and poloidal gap to allow flux to penetrate the shell. For times less than τ , the characteristic shell diffusion time, the shell stabilizes the plasma against MHD instabilities and holds the plasma in equilibrium via a distribution of induced current on the inner shell surface. For times much greater than τ , the equilibrium windings must provide the full equilibrium vertical field necessary to balance the hoop stress of the discharge column. In the interim, where the discharge time is comparable to τ , it is still necessary to provide a proper internal-external field match in order to minimize shell currents that can produce non-negligible field perturbations in the vicinity of shell ports and gaps. Hence, the equilibrium winding system must be able to track the plasma's state and provide a proper equilibrium on a time scale less than τ .

An analytic description of equilibrium field distributions applicable to a wide range of experimental configurations was initially proposed by Shafranov.^{1,2} The description employed the macroscopic equations of pressure balance for axisymmetric toroidal systems and resulted in, for large aspect ratios, the vertical magnetic field required for equilibrium. Although, in general, the equilibrium vertical field is a function of internal plasma parameters, the Shafranov results are insensitive to internal plasma structure and hence depend only on the macroscopic characteristics of the plasma column.

For a toroidal plasma discharge of major radius R and minor plasma radius a' , which denotes the innermost flux surface enclosing the total plasma current, the equilibrium vertical field for $\epsilon \ll 1$ is approximately given by¹

$$|B_{\perp}| = \frac{\mu_0 I \Phi}{4\pi R} \left[\ln \left(\frac{8R}{a'} \right) + \Lambda - \frac{1}{2} \right], \quad (1)$$

where

$\Lambda(a')$ = the asymmetry factor

$$= \beta_p(a') + \frac{k_1(a')}{2} - 1, \quad (2)$$

$$\beta_p(a') = \frac{2\mu_0 [\langle p \rangle - P(a)]}{B_z(a')^2}, \quad (3)$$

$$k_1 = \left(\frac{\mu_0}{4\pi} \right) k_1(a') = \left(\frac{\mu_0}{4\pi} \right) \frac{2 \int_{a'}^{R} B_p^2(r) r dr}{B_z(a')^2}, \quad (4)$$

$$B_0(a') = \frac{\mu_0 I \phi}{2\pi a'} \quad (5)$$

$\langle p \rangle$ denotes plasma pressure averaged over the plasma cross section; $P(a)$ denotes pressure at the vacuum vessel wall; I_0 represents the toroidal plasma current; B_p is the poloidal magnetic field; L_1 is the internal inductance; r , the integration variable, is the minor radial coordinate; and ϵ , the inverse toroidal aspect ratio, is equal to the ratio of minor to major radius of the shell.

In addition to providing equilibrium, stability, and radial positioning in the horizontal plane, the vertical field should also provide stability relative to displacement along the toroidal axis of symmetry (up-down drift). This constraint requires a vertical field-curvature such that discharge column displacements from the equatorial plane are countered by a radial component of the field that forces the column back to its initial position. The degree of field curvature may be quantified by the field index:

$$n = - \frac{R}{B_{\perp}} \frac{\partial B_{\perp}}{\partial R} \quad (6)$$

For $0 < n < 1.5$, the condition for vertical and horizontal stability is theoretically satisfied.

The Shafranov formulae have been checked for the case of an RFP plasma inside a conducting shell over a wide range of plasma conditions.³ In addition, Eq. 1 has been checked for several RFP configurations specific to the ZT-40U design where the plasma equilibrium is totally supported by the equilibrium windings. In both cases, the checks were performed by an axisymmetric, numerical Grad-Shafranov solver, and in both cases, the Shafranov formulae were accurate to within 5% of their numerical counterparts. Thus, Eqs. (1) through (6) provide a reasonable design specification for the ZT-40U equilibrium field control.

The Equilibrium Winding - (Equilibrium Control)

The equilibrium winding is responsible for maintaining plasma equilibrium over the duration of the discharge. The equilibrium winding must therefore provide a time varying vertical field and field index that tracks the plasma equilibrium [Eq. 1]. In addition, the equilibrium winding must also satisfy design constraints to:

- 1) Maximize physical access to the torus for maintenance, vacuum pumping, and plasma diagnostics.
- 2) Minimize the applied power necessary to control the equilibrium field.
- 3) Minimize axisymmetric field errors in the discharge chamber. The deviation of a plasma flux surface ($\delta\psi$) due to axisymmetric errors should remain less than 4% of the minor toroidal radius in order to minimize the intersection of an outer plasma flux surface with the discharge vacuum vessel.

A cross sectional diagram of the resulting equilibrium coil system is shown in Fig. 2. The winding consists of eight discrete coils that are each

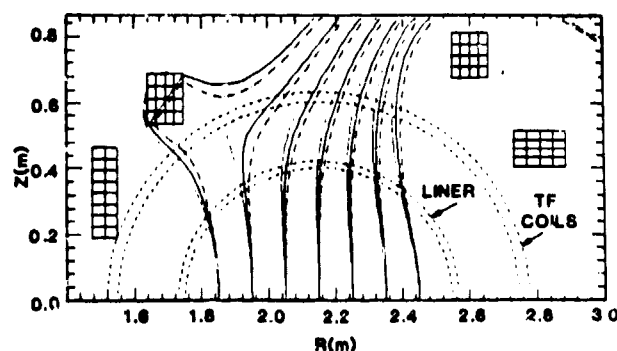


Fig. 2. Equilibrium winding vacuum vertical field for three field indices. ($n = 0.2, 0.5, 0.8$ [from left to right]).

composed of multiple turns and are symmetric about the equatorial plane.

As previously noted, most of the equilibrium vertical field is inductively driven by the plasma. However, because the EF coil-liner spacing is large, this induced current provides only 70% of the required equilibrium field during the 20 msec plasma current rise. As a result, the EF coils are configured to boost the induced current by utilizing the magnetizing flux. In this way, the power required to track plasma equilibrium during the current rise and flat top regions of operation is maintained at a reasonable level.

Figure 2 illustrates the vacuum vertical field produced by the equilibrium winding for three different field indices. In all cases, the field and field curvature are relatively constant over the discharge volume.

The Magnetizing Winding - (Discharge Driver)

The magnetizing (M) winding is responsible for driving the plasma discharge. Therefore, it must supply both the flux swing and stored magnetic energy necessary for initiating and sustaining the discharge current. Operationally, this is accomplished by precharging the M winding via a power supply, and then discharging the winding across a transfer resistor. The changing magnetizing flux due to discharging induces the toroidal plasma voltage that drives the discharge current.

The amount of M-winding flux swing available for driving the discharge is critical, since it ultimately determines machine performance from the stand point of current magnitude and duration. The required poloidal flux input for a 2 MA discharge may be estimated by scaling flux consumption measurements from the ZT-40U experiment. Recent measurements project between a 9.2 and 11.9 volt-second consumption for risetimes between 10 and 20 ms, respectively.⁴ These projections probably represent conservative estimates.

A cross sectional diagram of the M coil system is illustrated in Fig. 1. The M winding consists of 16 discrete coils that are each composed of multiple turns (160 total) and are symmetric about the equatorial plane. The winding configuration incorporates design constraints to:

- 1). Maximize physical access to the torus.

2. Maximize electrical transfer efficiency between the M-winding and the plasma.
3. Minimize axisymmetric field errors in the plasma due to flux leakage.

Simple numerical programs using elliptic integrals were composed to calculate fields, flux surfaces, inductances and coil forces. The input parameter file format for these programs were identical so that the files could be passed between mechanical, circuit, and magnetics designers in an iterative process. A program was also written to calculate coil positions for minimum magnetic field magnitude within the liner under specified constraints. After several sets of iterations, in which the energy transfer efficiency was calculated using the SCEPTRE circuit code as a coupled RFP O-D model¹, a transfer efficiency of 12% was obtained. The final magnetizing winding design produces a hexapole null at the minor axis and 130 gauss vertical field at the plasma liner for 35 kG on the major axis at the midplane. This error meets the 4% flux surface deviation criterion. When fully excited (5.4 MA turns), the winding stores 86 MJ and 15.8 V-sec (Wb). Figure 1 shows a flux plot for full current operation.

Numerical Poloidal Field System analysis

The poloidal field system must provide equilibrium over two distinct time frames. For times short compared to the characteristic diffusion time of the shell, equilibrium is provided by shell currents. In addition, the shell shields the plasma from axisymmetric errors and field ripple generated by the discrete external field windings. Hence, the equilibrium magnetic flux surfaces have approximately nonconcentric circular cross sections. RFP equilibria in the presence of the conducting shell have been extensively studied by numerical computation.³

For times comparable to or longer than the shell diffusion time, plasma equilibrium is supported by the equilibrium windings. For this case, the equilibrium properties of the poloidal field system were checked by a code that numerically solves the Grad-Shafranov equation in the presence of fixed, current carrying conductors. Code input required the spatial location of each magnetizing and equilibrium coil, the total current in each coil, and a poloidal flux function and pressure profile representative of the predicted ZT-40U performance.

The code results are illustrated in Fig. 3. The computations indicate that winding controlled equilibria are physically viable for the proposed poloidal field system. The equilibrium coils are capable of controlling the plasma equilibrium over the range of expected plasma Λ ($\sim 0.7 < \Lambda < 0.2$). Also, total flux surface distortion due to the discrete magnetizing and equilibrium windings remained less than 4% of the minor toroidal radius.

Coil Crosssection, Turns, Minimum Error Field

For the magnetizing windings, eight coil groups of twenty turns each are selected to provide 10 volt seconds to the plasma with a 20-millisecond risetime. The total 10.8 MA turns are divided by the current density value of 30 MA/m² to arrive at the required copper area of 22.6 cm² (3.5 in²). A current density between 25-30 MA/m² achieves a balance between total energy cost, permissible temperature rise and copper cost. The resulting terminal current is 67.5 kA. The average copper cross section needed for one poloidal coil turn was found to be 0.67 in²/turn based on the average coupling current of 15 kA/turn, and a current

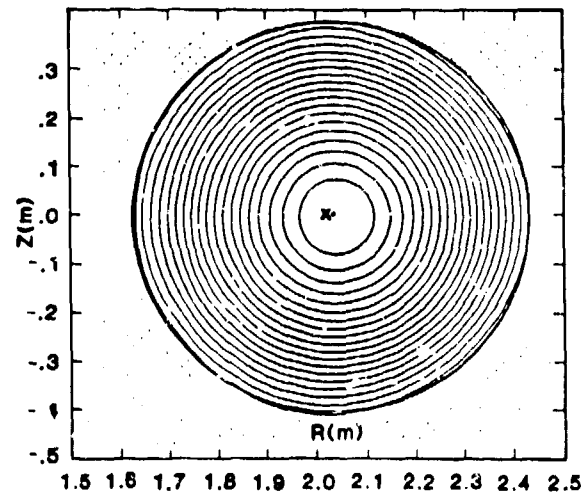


Fig. 3. The equilibrium poloidal flux contours. The (x,.) denote the position of the (geometric, magnetic) axis, respectively.

density of 35 MA/m². The dimensions of the copper conductor are a function of the coil winding sequence, the space allocated by the structural layout, and the insulation requirements.

Computer aided design was used to develop -

- a) The most effective placement of crossover segments in the winding sequence for minimum field error,

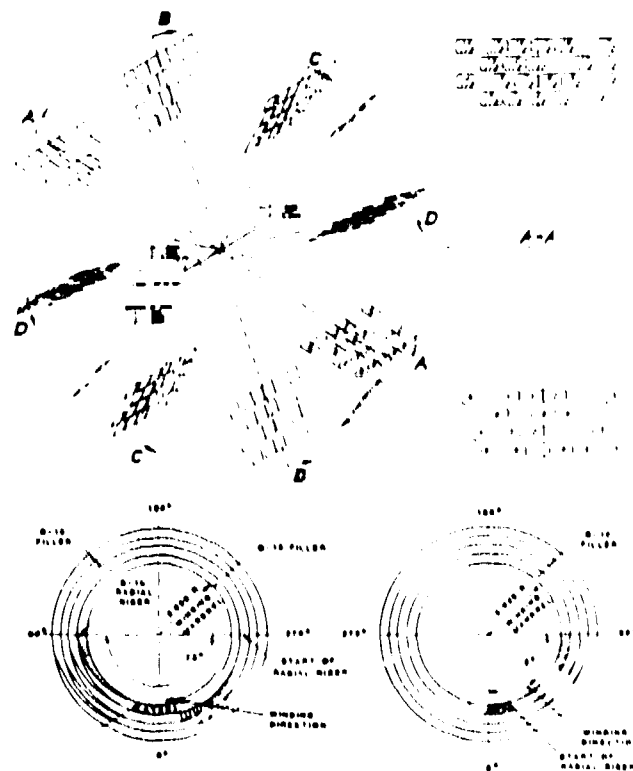


Fig. 4. Coil Current Center and Tilt Angle by Computer Aided Design.

- b) The location of the current center along the X,Y,Z axis and tilt angle.

The number of turns per coil is determined by a balance between risetime and the maximum allowable voltage for turn-to-turn coil insulation. For low energy consumption and high flux coupling, it is desirable to have the coils as close as possible to the plasma, but positioning the coils further away from the plasma reduces the magnetic field error. Computer codes were developed to predict a reasonable coil configuration resulting in a low field error. (See Table I)

Coil Stresses & Cooling

The combined principal stresses due to hoop and bending for every coil configuration are calculated and compiled by computer code. The program takes into account the parameters of width, depth, and location of each coil, the length between supports, and the current to be carried by each coil. The magnetizing current force vector is directed toward the plasma, and because the thermal stress in some instances is additive, it becomes desirable to limit the combined hoop and bending stress to 12,000 psi. Choosing 1/4 hard, CD-104 copper with an ultimate stress of 30,000 psi allows a design stress of 15,000 psi and provides a thermal stress margin of 3,000 psi.

Hoop and shear stresses were determined for each of the magnet systems by investigating the superimposed effects of hoop bending and thermal stresses under specified support conditions.

- a) The hoop stress, caused by the magnetic pressure from the axial magnetic fields, was calculated by using the normal thin shell approximation:

$$S = \frac{PD}{2t},$$

where:

$$P = \text{magnetic pressure} = \left(\frac{B^2}{2\mu_0} \right) = \frac{\mu_0 I^2}{8\pi^2 r^2} \text{ Newtons/meter}^2$$

S = hoop stress,
D = coil mean diameter,
t = coil thickness,
B = magnetic field at coil bore.

- b) The bending shear stress between supports, caused by vertical magnetic fields, and the weight of the coils is determined by:

$$S = \frac{Mc}{I},$$

where I/c = the section modulus of the conductor cross section, and M = the bending moment; a function of length between supports.

TABLE I

MINIMUM MAGNETIC ERROR FIELD AT VACUUM CHAMBER					
Angle	B	B _z	B _r	B _θ	B _φ
180.0	125.8	0.736E-04	-125.8	-0.1357E-03	-125.8
193.0	129.7	.76.9	-104.5	105.4	-75.6
216.0	135.5	-129.3	-40.4	128.4	43.3
234.0	135.2	-125.7	48.9	33.5	131.0
253.0	133.8	-59.3	120.0	-35.8	33.4
270.0	136.1	33.3	131.9	-131.3	-33.3
288.0	135.7	105.6	85.2	-48.5	-126.7
306.0	131.6	131.3	8.6	70.2	-111.3
324.0	129.3	111.3	-64.9	128.6	-13.8
343.0	130.4	62.6	-114.4	94.8	89.5
360.0	131.5	0.2002E-03	-131.5	0.3234E-03	131.5

A computer code was developed to arrive at the actual combined hoop and bending stresses under conditions which satisfied the placement of the coils and the structural design of the support frames. (See Table II)

- c) The compressive stresses which occur at structural restraints as a result of thermal expansion were evaluated, and their values superimposed on hoop and shear stresses. Since the temperature rise is a function of the time duration of the pulse, it is instructive to determine the thermal stress in the restrained direction caused by heat input to the system, assuming an adiabatic system:

$$\text{Temperature rise} = \Delta T = \frac{\rho J^2 t}{(U.C.)\gamma},$$

$$S_T = \text{thermal stress} = E \alpha \Delta T,$$

$$\text{Thermal stress/time} = s/t = \frac{E \alpha \rho J^2}{U.C. \gamma},$$

where:

E = Young's modulus,
α = Coefficient of expansion,
ρ = resistivity,
J = current density,
U.C. = specific heat,
γ = density.

In a typical case the current density in a copper conductor might be 20 MA/m². If this flows for five seconds, the temperature rise would be 15.5°C (3.1°C/s), and the thermal stress in a restrained section would be 25.3 MPa (3668 psi).

- d) In considering the cooling of the conductor, it is important to note that a balance must be achieved between the temperature rise of the copper and the cooling water, and that this be done over the length of the cooling path. A modified version of the Princeton "Kencool" program calculates (ΔT) values under pulse conditions for given values of inlet water and coolant hole; copper length and area; equivalent square wave and repetition cycle; and current (kA/turn) and flow rate. The code calculates temperatures of copper and water for approximately one hour of operation until the temperature values converge. For the magnetizing windings, the equivalent square wave equals 4.2 sec, and the duration of the repetition rate equals 300 sec. (See Table III)

- e) Interlaminar shear was calculated assuming that the copper and insulation are well bonded, and therefore the composite of copper and insulation would have to expand as a unit. On that basis, an average coefficient of expansion was calculated for the composite. To find the differential strain between copper and insulation, it was necessary to compute separately the virtual thermal expansion of every component: the composite member, the copper, and the insulation, each without restraint, and then solve for the force which acts on the bonded interface between

TABLE II

COMBINED HOOP AND BENDING STRESSES IN THE COIL

	R IN	Z IN	NI A	PZ LB	PR L LB IN	PZ L LB IN	HOOP COMBINED STRESSES PSI
1	44.00	4.20	8.10E+06	2.07E+06	1.08E+04	7.47E+02	1.00E+04 1.11E+04
2	46.00	13.00	8.10E+06	6.83E+06	9.87E+03	2.00E+03	1.06E+04 1.12E+04
3	47.75	22.27	8.10E+06	8.06E+06	7.93E+03	2.80E+03	8.80E+03 1.01E+04
4	50.00	32.00	8.10E+06	1.51E+06	8.87E+03	4.74E+03	8.00E+03 1.05E+04
5	51.00	42.41	8.44E+06	7.87E+06	2.31E+03	2.00E+03	4.80E+03 7.85E+03
6	76.81	66.76	8.44E+06	6.31E+06	2.02E+03	1.31E+03	5.00E+03 8.10E+03
7	94.80	83.47	8.44E+06	6.45E+06	7.10E+02	8.18E+02	2.20E+03 7.40E+03
8	123.90	98.46	8.44E+06	5.96E+06	8.22E+01	6.11E+02	3.30E+02 6.00E+03

TABLE III

COIL COPPER AND COOLING WATER TEMPERATURE GRADIENTS

START			
TIME: 603.068 SECONDS			
CONDUCTOR TEMPERATURE			
46.8 50.0 54.1 58.2 62.1			
RES (MILLIOHMS) 0.396			
Inlet Water 28.000 Degrees C			
TIME: 898.526 SECONDS			
CONDUCTOR TEMPERATURE			
27.1 30.3 34.6 39.1 43.7			
TIME: 1790.526 SECONDS			
CONDUCTOR TEMPERATURE			
27.1 30.4 35.0 39.7 44.8			
WATER TEMPERATURE			
23.2 25.8 29.1 33.0 37.4			
RES (MILLIOHMS) 0.369			
FINISH			
TIME: 1790.526 SECONDS			
CONDUCTOR TEMPERATURE			
27.1 30.4 35.0 39.7 44.8			
WATER TEMPERATURE			
23.2 25.8 29.2 33.3 38.0			

copper and insulation in the form of shear. The resulting stress, which is equivalent to the force over the bonding surface, has in each case been less than the allowable value of 20.7 MPa (3000 psi) documented by experimental data from various sources.

The Upper Structure

The upper structure consists of beams, columns and plates which support the weight and forces of the magnetizing coils and also the access platform. The structure is composed of twelve modular pie-shaped sections bolted together at assembly. Figure 5 illustrates one of the 30° modular sections. The bulkhead-pedestal structure supports the vacuum shell and the poloidal and toroidal coils. The structure is sectioned to allow access, assembly, and removal of the coils and other components.

Because of the complexity of the upper structure and the number of interacting forces, a finite element analysis was initiated to confirm stresses and deflections in the fiberglass frame. Only one of twelve bulkhead frames (or the equivalent of a 30°

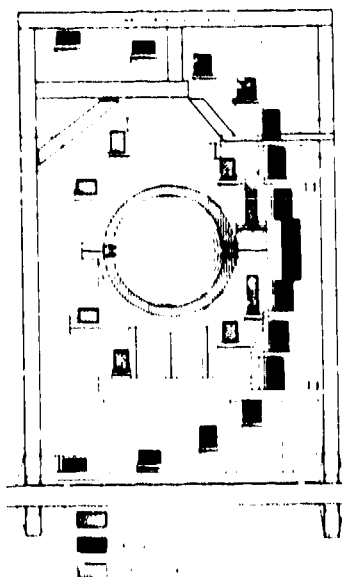


Fig. 5. Cross-sectional view of structure, liner and coil positions.

segment of the support structure) needed to be considered by the computer model, because all the loads are repetitive and axi-symmetric about the torus centerline.

The Loads

The loads used in the analysis were based on full current in all the field coils, the 160,000 lbs. weight of all the components, vacuum on the liner and the toroidal coil centering force and toppling moment. Loads due to the thermal expansion of the coils were not considered, and the coils were modeled as rectangular copper sections without giving structural credit to the epoxy-fiberglass insulation. Weight effects of structural members and the direction of gravity acceleration were included in the analysis. The maximum magnetic forces on the magnetizing coils are given in Table IV. The magnitude and direction of the magnetizing coil vectors form a major part of the loading in the finite element model.

TABLE IV

NORMAL FORCES ON MAGNETIZING COILS AT PEAK CHARGE
($I_m = 136$ kA)

Coil No.	θ Degrees	F/1 (lb/in.)
M1	-6	9,970
M2	-25	10,960
M3	-9	8,960
M4	-38	5,330
M5	-22	3,530
M6	-22	2,960
M7	-64	2,470
M8	-67	560
M9	-91	340
M10	-148	230

Boundary Conditions and Method of Analysis

The base of the upper support frame was thought of as being fixed at the inner and outer radii. At these locations, the frame is attached to another platform, which in turn is fastened to the concrete floor below. The nodes on the $\pm 15^\circ$ planes of symmetry were considered to be restrained from translating normal to the plane, and from rotating in the plane of symmetry. The joints in the frame (beams, columns and plates) were assumed to be rigid. The fiberglass plate material was construed to be isotropic in plane.

Linear theory was deemed appropriate. The finite element linear theory program reduces the structural components into small elements. A closed-form solution is performed on these elements to evaluate their structural properties or stiffness. The stiffness of the entire structure is then modeled by assembling the stiffnesses of all the elements into a stiffness matrix for the structure. The displacements of the overall structure can be computed by using the appropriate forces and by applying matrix algebra.

Design Description

Stresses resulting from the finite element code appear to be in good agreement with independent calculations, and the deformed mesh rendered a clear critique of the original design, calling for increased moment of inertia for some of the structural members. The results of the model are shown and summarized in Fig. 6 and Table 5. The largest deflection, 0.3 inches, occurs in the upper corner of the structure, and is attributed to the weight and coil forces of the

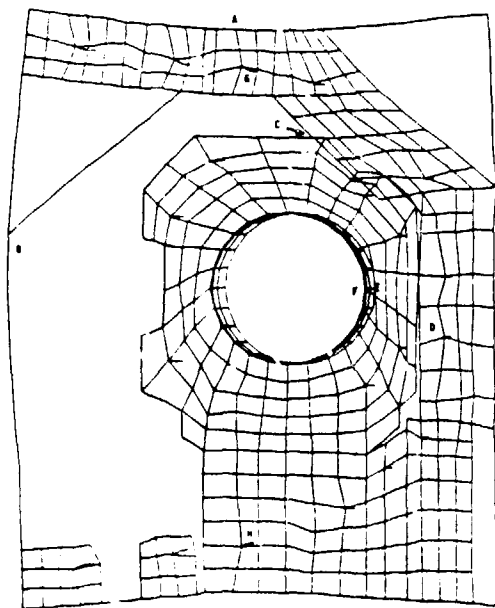


Fig. 6. Scaled-up Deflection of Finite Element Model.

TABLE V
DEFLECTION & STRESSES FROM THE FINITE ELEMENT ANALYSIS
MATERIAL PROPERTIES

Material	Young's Modulus (10 ⁶ psi)	Poisson's Ratio	Density (lb/in. ³)	Tensile Strength (ksi)
G-10 (plates)	2.0	0.25	0.065	50
Extren (beams)	2.0	0.25	0.065	25
Copper (coils)	17.0	0.33	0.320	30 (yield)
Aluminum (torus)	10.5	0.30	0.097	30 (yield)

UPPER SUPPORT STRUCTURE RESULTS

Region Description	Defl. Stress	Material
Top of frame	0.3 in. vert.	Fiber glass
Outside of frame	0.2 in. horiz.	Fiber glass
Frame bulkhead interference	0.25 in. vert.	Fiber glass
Inside of frame	13 ksi (Beam)	Extren
Inside of frame	11 ksi (plate)	G-10
Torus bulkhead attachment	2 ksi (Plate)	G-10
Torus	7 ksi (Plate)	Aluminum
Magnetizing coils 8 and 18	16 ksi (Plate)	Copper
Magnetizing coil 8	0.33 in. vert.	Copper

magnetizing windings. A redesign will minimize deformations by

- increasing beam depth,
- splice connecting G-10 plates into one continuous structure,
- adding deep crosssection gussets in the corners of the upper frame.

The 360° cage type structure created by connecting all of the frames with all of the bulkheads and the toroidal shell (Fig 7) will provide added rigidity needed to achieve minimum deflection.

References

- [1] V. D. Shafranov, "Plasma Equilibrium in a Magnetic Field," in *Reviews of Plasma Physics V2*, edited by M. A. Leontovich (Consultants Bureau, New York, 1966), P. 103-151.
- [2] V. S. Mukhavatov and V. D. Shafranov, "Plasma Equilibrium in a Tokamak," *Nucl. Fusion* **11**, 605 (1971).
- [3] D. A. Baker, L. W. Mann, and K. F. Schoenberg, "Equilibrium Poloidal Field Distributions in Axisymmetric RFP Toroidal Discharges," *Nucl. Fusion* **23**, 380 (1982).
- [4] K. F. Schoenberg and J. A. Phillips, Los Alamos National Laboratory, private communication (1982).
- [5] K. F. Schoenberg, R. F. Gribble, and J. A. Phillips, "Zero-Dimensional Simulations of Reversed Field Pinch Experiments," *Nucl. Fusion* **22**, 1433 (1982).
- [6] S. Timoshenko, *Theory of Elastic Stability*, (McGraw-Hill Book Company, New York, 1936).
- [7] P. F. Jordon, "Buckling of Toroidal Shells Under Hydrostatic Pressure," *AIAA Journal* (October 1973).
- [8] L. H. Sobel and W. Flugge, "Stability of Toroidal Shells Under Uniform External Pressure," *AIAA Journal* (March 1967 and November 1969).
- [9] R. J. Roark, *Formulas for Stress and Strain*, 4th Edition (McGraw-Hill Book Company, New York, 1965) p. 343.
- [10] K. E. Wakefield, Princeton Ken-Cool program for Temperature Rise in Conductor and Cooling Water During Pulse Conditions.

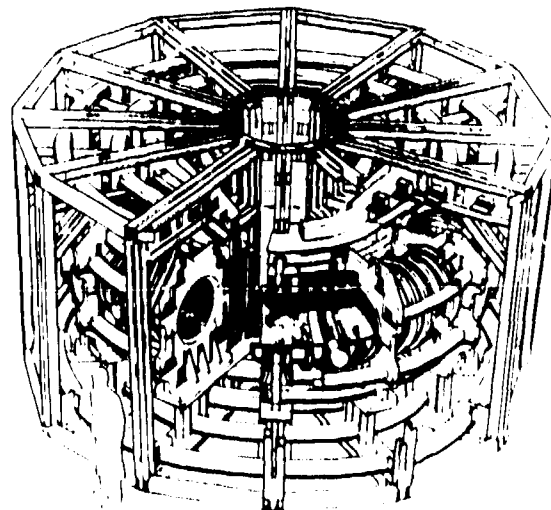


Fig. 7. Isometric View of ZT-40 Upgrade